Coalescence of Immiscible Polymer Blends in Chaotic Mixers

Jairo E. Perilla and Sadhan C. Jana
Dept. of Polymer Engineering, The University of Akron, Akron, OH 44325

DOI 10.1002/aic.10500
Published online July 18, 2005 in Wiley InterScience (www.interscience.wiley.com).

The study evaluated if excellent mixing conditions prevailing in chaotic mixers also promote droplet coalescence in the mixing of immiscible polymers. A combined approach of experiments and simplified modeling was used to understand the effects of the degree of chaotic mixing, shear rate, and viscosity ratio on coalescence rates. It was found experimentally that the extent of coalescence was substantially reduced when the bulk of the fluid in the mixer experienced chaotic mixing. In addition, coalescence was subdued at higher rates of shear and for higher viscosity ratio droplets. Pseudo-steady state droplet size distributions were reached faster with higher droplet volume fractions and for higher viscosity ratio droplets. © 2005 American Institute of Chemical Engineers *AIChE J,* 51: 2675–2685, 2005
Keywords: coalescence, chaotic mixing, flow reorientation, immiscible polymers, collision.

Introduction

In processing of immiscible polymers, such as dispersive mixing in extruders, injection molding, and profile extrusion, a common goal is to generate and maintain the dispersed phase to the smallest possible size to achieve uniform properties, for example, impact toughness, dimensional stability at higher temperatures, and optical clarity.[1] Prior work on mixing of immiscible polymers in screw extruders revealed that morphology development begins with deformation of the dispersed phase into lamellas, followed by formation of fibrils and droplets.[2-6] The droplets, if over a critical size, repeat the same process of deformation and breakup, and generate a population of even smaller droplets. The critical droplet size is determined from the values of interfacial tension (Γ), viscosity ratio (p), shear rate $\dot{\gamma}$, and viscosity of the continuous medium (η_c) and is often estimated from the value of the critical capillary number

$$Ca_c \equiv \frac{R_c \eta_c \dot{\gamma}}{\Gamma} \tag{1}$$

where R_c is the critical radius of the droplet. The relationship between Ca_c and viscosity ratio p can be obtained from a series of experiments on drop deformation and breakup, as was obtained by Grace[7] for Newtonian fluids. Droplets smaller than the critical size do not break up but undergo coalescence. Accordingly, morphology evolution during polymer mixing continues until a steady-state droplet-size distribution is reached, at which point, the rate of droplet breakup is comparable to that of droplet coalescence. DeRoussel et al.[8] showed that the steady state can be approached either monotonically or through a state of over-emulsification where the average size oscillates about a mean diameter. Some investigators[9-10] also reported hysteresis in droplet size, for example, the steady-state morphology differed depending on whether the steady state was approached from the smaller or from the larger size droplets.

It has been recently demonstrated that chaotic flows provide excellent means for producing fine scale dispersed phase morphology in the blending of immiscible polymers.[11-16] In these studies, repeated alignment, stretching and folding of the fluidic interfaces produce self-similar mixing structures which

Correspondence concerning this article should be addressed to S. C. Jana janas@uakron.edu.

© 2005 American Institute of Chemical Engineers

acted as templates for a series of morphological transitions similar to what was observed in nonchaotic flows,[2-6] for example, lamella, fibrils, droplets and their combinations, but with much smaller length scales. The chaotic fluid element trajectories also enhance transport of mass and energy[17-22] and improve distributive mixing in single screw extruders.[23-24] A natural question comes to mind if chaotic mixing flows also promote coalescence of the dispersed droplets, especially in light of more frequent collisions expected. This question was investigated in this study by allowing premade blends of two immiscible polymers to coalesce under chaotic flow conditions. The shear rates were chosen such that the droplets underwent only coalescence and not breakup. The results of this study is expected to provide insight for development and optimization of chaotic mixers for processing of polymer blends and emulsions and in the design of modular mixing elements for screw extruders and molding devices.

Steps in coalescence

Coalescence has been described in the literature[25-27] as a compound of three independent, successive events: (a) approach of the droplets, (b) interaction between the droplets and drainage of the fluid separating the droplets, and (c) relaxation of the two-droplet dumbbell into more stable spherical shape. In an "effective" collision, the fluid between the droplets drains out, the drops join by the action of the van der Waals forces, and the composite drop relaxes to form a new spherical globule. In this context, the periodic flow reorientation encountered in chaotic flows is anticipated to alter the rate of collision and to reduce the time available for drainage as the droplets diverge from each other in chaotic flows.

Droplet collision frequency due to Brownian motion is low[28-29] and increases significantly in the presence of imposed flows.[25, 27] Recently, a study was undertaken in our laboratory, where the time-scales of droplet approach and fluid drainage were compared and the extent of coalescence in model polymer processing flows was analyzed.[30] Some studies also reported the effects of mixing on coalescence.[31-34] Droplet coalescence in chaotic mixing flows has not been studied previously, although Muzzio and Ottino[35] predicted increased rate of coagulation of massless tracer particles in a model chaotic flow, that of blinking vortex system.[36]

In this work, we first investigated, using simplified models, coalescence of equal size droplets suspended in a continuous fluidic medium subjected to simple shear flow. The direction of shear was changed time-periodically with a prescribed frequency. The results were analyzed in terms of the number of flow reorientation periods necessary to obtain coalescence for a given value of reorientation angle. Next, we carried out a series of experiments on coalescence of premade droplets in chaotic flows and analyzed the data to assess the influence of the degree of chaotic mixing, viscosity ratio of the polymer components, composition, and the mean shear rate in the mixer on the rate of coalescence.

Flow reorientation, droplet mixing, and coalescence

Figure 1 shows a model, two-droplet system of radius R undergoing coalescence in a simple shear flow of shear rate $\dot{\gamma}$. One droplet remains at the center of the coordinate frame and

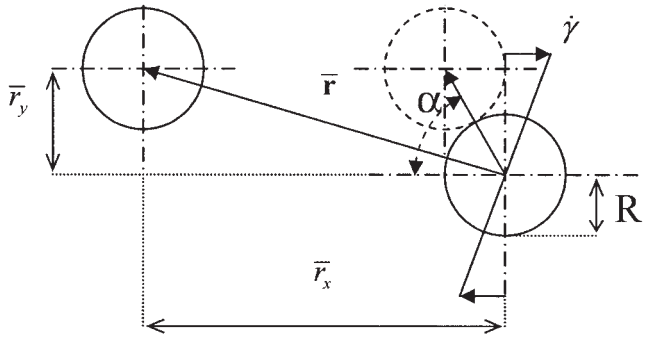

Figure 1. Two-droplet system in simple shear flows.

the other approaches from an initial distance, $|\bar{\mathbf{r}}|$, where $\bar{\mathbf{r}}(\bar{r}_x, \bar{r}_y)$ is the vector joining the centers of the droplets. The fastest approach is observed when the incident droplet approaches along the streamline separated by a distance $\bar{r}_y = 2R$ (see Figure 1). On the other hand, collision does not occur if the droplets travel along the same streamline. An average value of collision frequency C, the number of collisions per unit volume, is obtained by considering all the collisions taking place between $\bar{r}_y = 0$ and $\bar{r}_y = 2R$, as given below by the Smoluchowski equation[37]

$$C = \frac{16}{3} n^2 \dot{\gamma} R^3 \tag{2}$$

In Eq. 2, n is the number of droplets per unit volume, and $\dot{\gamma}$ is the macroscopic shear rate. If the direction of shear flow is changed periodically, the approaching droplet changes the course of the motion with a frequency, the same as that of frequency of flow reorientation. Consequently, the droplets do not remain on the original trajectories as depicted in Figure 1 after flow reorientation. On the other hand, many droplets initially not expected to undergo collision, for example, those with $|\bar{r}_y| > 2R$, can follow pathways leading to collision after flow reorientation. Figure 2 shows how flow reorientation can be implemented in conjunction with simple shear flows. It consists of four steps: (a) simple shear flow with shear rate $\dot{\gamma}$ applied for a time period, $\tau/2$, (b) the flow field reoriented at an angle β, (c) the simple shear flow applied for a time period $\tau/2$, and finally (d) the flow is reoriented back to the initial direction. In view of this, the evolution of the normalized vector $\mathbf{r}$

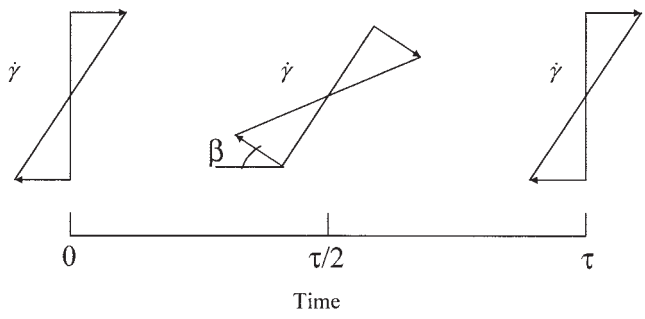

Figure 2. Model for flow reorientation period in simple shear flows.

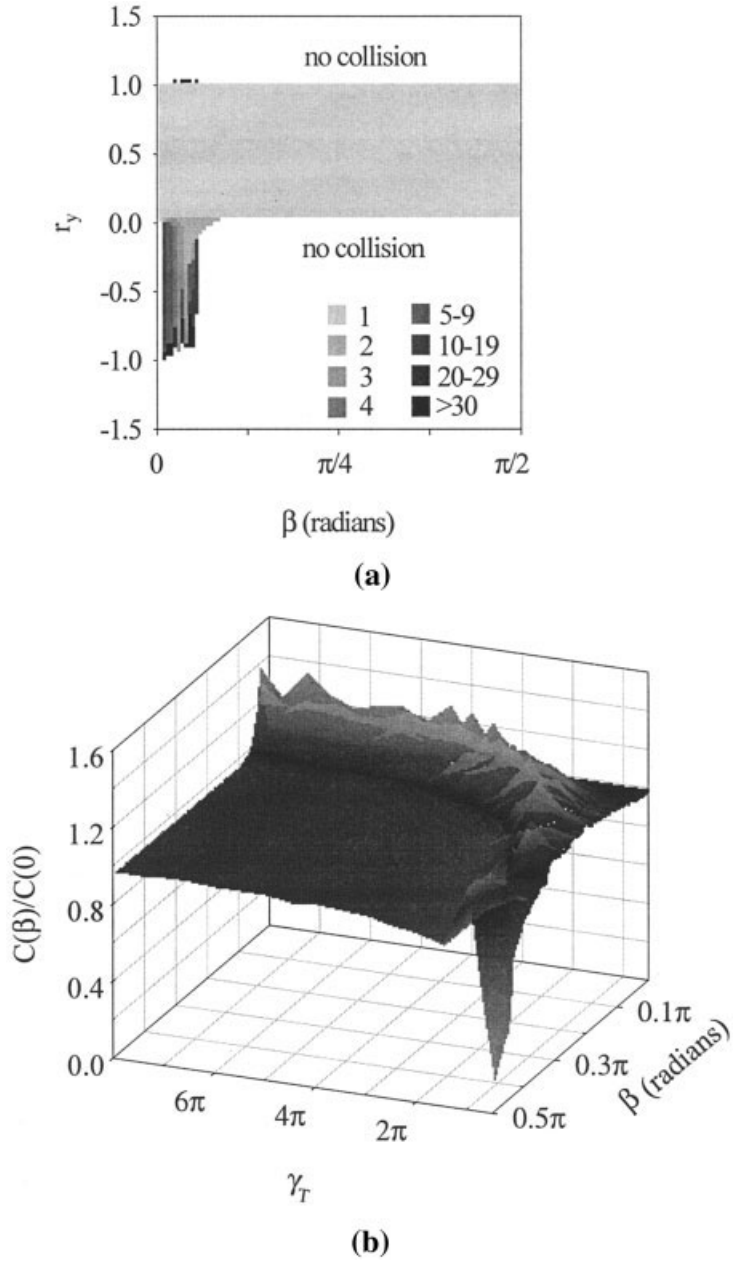

Figure 3. (a) Number of reorientation periods (gray-scale code) necessary for collision $\gamma_T = 8\pi$, $\phi = 0.15$, and (b) normalized number of collisions per period, C(β)/C(0), vs. reorientation angle, β, and γ_T for a two droplet system in simple shear flow.

$\equiv \bar{\mathbf{r}}/2R$ during one reorientation period, τ can be written as follows

$$r_{x1} = r_{y0}\gamma_T/2 + r_{x0}; \quad r_{y1} = r_{y0} \tag{3}$$

$$r_{x2} = r_{x1}\cos\beta - r_{y1}\sin\beta; \quad r_{y2} = r_{x1}\sin\beta + r_{y1}\cos\beta \tag{4}$$

$$r_{x3} = r_{y2}\gamma_T/2 + r_{x2}; \quad r_{y3} = r_{y2} \tag{5}$$

$$r_{x0} = r_{x3}\cos(-\beta) - r_{y3}\sin(-\beta); \quad r_{y0} = r_{x3}\sin(-\beta) + r_{y3}\cos(-\beta) \tag{6}$$

where r_x and r_y are the x- and y-components of $\boldsymbol{r}$, γ_T corresponds to the strain per period ($\gamma_T = \dot{\gamma}\tau$), and the subscripts 0, 1, 2, and 3 represent the conditions at the beginning of the period $\tau/2$, after shearing for a time $\tau/2$, after flow reorientation, and after shearing for the other half period $\tau/2$, respectively. It is important to note that only the direction and not the magnitude of $\boldsymbol{r}$ changes due to flow reorientation. Equations 3

– 6 can be solved for the number of periods necessary to effect the collision, that is, to obtain droplets with $|\mathbf{r}| \leq 1$, or to accept the divergence of the trajectories if $|\mathbf{r}| > 1$ and, therefore, no collision. Figure 3a presents collision maps using initial separation $|\mathbf{r}| = (\pi/6\phi)^{1/3}$ with ϕ as the volume fraction of the droplets. In Figure 3a, the number of periods necessary for a collision to take place is presented as function of the position (r_y) of the second droplet and the value of β, for a value of strain per period, $\gamma_T (\equiv \dot{\gamma}\tau) = 8\pi$. A band appears where the collision occurs within the first reorientation period ($n = 1$); the size of this band is almost insensitive to the value of β, Figure 3a. In this case, the incident droplets travel a relatively long distance in a period $\tau/2$, before undergoing reorientation. Consequently, many droplets in Figure 3a have collided as if in a flow with no change in the direction of shear ($0 < r_y < 1$), and, thus, β has no effect. The increase of droplet collision due to flow reorientation is apparent only for $\beta < 0.25$ radians; however, these collisions require a large number of periods. Note also that droplets, falling outside the regular collision zone ($0 < r_y < 1$), do not collide at all, as their trajectories diverge at large values of β.

The number of collisions per reorientation period, $C(\beta)$ which is a function of the reorientation angle, β, as $C(\beta) = \Sigma 1/$(periods per collision at r_y), can be computed from the data presented in Figure 3a. Figure 3b shows the values of $C(\beta)/C(0)$ as function of γ_T and β, where $C(0)$ is the value of C with no reorientation. Note that normalization of $C(\beta)$ with $C(0)$ is necessary in order to compare the effects of γ_T and β. Figure 3b indicates that for smaller values of β, $C(\beta)$ increases with β, but at a certain value of β, it equals the collision frequency of the unoriented case and then decreases again. A continuous decrease is observed for $\pi/2 \leq \gamma_T \leq \pi$, while the ratio $C(\beta)/C(0)$ reaches a plateau for $2\pi \leq \gamma_T \leq 8\pi$ at values smaller than unity. Thus, flow reorientation is effective in reducing the collisions when $\beta \geq \pi/3$ and most effective when $\beta = \pi/2$. On the other hand, smaller values of β promote collisions, $C(\beta)/C(0) > 1$, although, as will be seen, not all collisions lead to coalescence. At smaller values of γ_T, the droplets collide after the flow undergoes several flow reorientations. This is readily apparent for $\gamma_T = \pi/2$ (Figure 3b). For values of $\beta < \pi/3$, much larger number of collisions are required than in unoriented case. Collision is gradually reduced for larger values of β, until it is totally suppressed for $\beta = \pi/2$. However, low values of γ_T are not practical in mixing operations as these conditions produce poor mixing.[38-40] Note that periodic flow reorientations are effective in producing good mixing when large values of β and γ_T are used. In addition, for a given β, mixing is significantly improved at higher values of γ_T.

A collision can finish in coalescence if the contact time is larger than the time of drainage. Otherwise, droplets separate out before coalescing. The time of drainage is obtained by solving the equations of continuity and motion in the liquid film separating the droplets, for example, using boundary integral method[41] and finite difference method.[42] In this contribution, an approximate solution, based on partially mobile interfaces[26, 42] is used. The rate of thinning of the fluid film is given by Janssen and Meijer[26]

$$\frac{dh}{dt} = -\frac{2h^2(2\pi\Gamma/R)^{3/2}}{\pi\eta_d F^{1/2}} \tag{7}$$

where h is the smallest thickness of the fluid film at any time t, F is the drag force, Γ is the interfacial tension, and η_d is the viscosity of the droplet fluid. The drag force is obtained from Allan and Mason[43]

$$F = 4.34\pi\eta_c R^2\dot{\gamma}\sin 2\alpha \tag{8}$$

$$\frac{d\alpha}{dt} = \dot{\gamma}(0.8\cos^2\alpha + 0.2\sin^2\alpha) \tag{9}$$

where α is the angle of contact (see Figure 1), formed between the direction of shear flow and the line joining the centers of the droplets, and η_c is the viscosity of the continuous fluid. In this article, η_c is assumed independent of the rate of shear. The time for drainage is obtained from integration of equation 7 between the limits h_0 and h_{cr}. Here, h_0 represents the distance at which the approaching droplet feels the presence of the other, and beyond h_{cr}, the van der Waals forces produce the fusion of the droplets and coalescence. The values of h_0 and h_{cr}[26] can be normalized by the droplet radius R as follows

$$\frac{h_0}{R} = 0.6069(\sin 2\alpha)^{0.75} Ca^{0.75} p^{0.5} \tag{10}$$

$$\frac{h_{cr}}{R} = \left(\frac{A}{8\pi R^2\Gamma}\right)^{1/3} \tag{11}$$

Here Ca is the capillary number, $\mathrm{Ca} = \dot{\gamma}\eta_c R/\Gamma$, p is the viscosity ratio ($p = \eta_d/\eta_c$), and A is the Hamaker constant; A includes all the effects of the van der Waals forces.[44] Equations 7 – 11 can also be used to obtain an expression relating the contact angle at collision α_0, and the contact angle at coalescence α_1. In view of this, a critical angle of collision ($\alpha_0 = \alpha_{cr}$)[32] can be found by taking $\alpha_1 = \pi/2$. It is assumed that coalescence is complete when the droplets fuse together to form a dumbbell. The dumbbell relaxes to a larger spherical droplet. For $\alpha > \alpha_{cr}$, collisions do not lead to coalescence as the time required for drainage is longer than the time of contact. In view of this, the frequency of effective collisions can be calculated from equation 2 by introducing an efficiency factor P_{12} which is the ratio of the area of the droplet where the collisions are effective ($0 < \alpha \leq \alpha_{cr}$) to the total area where collisions can take place ($0 < \alpha < \pi/2$) as expressed in Eq. 12

$$P_{12} = 3\int_0^{\alpha_{cr}} \cos^2\alpha \sin\alpha d\alpha \tag{12}$$

In view of this, the frequency of effective collisions, C_{eff}, can be defined as

$$C_{eff} = CP_{12} \tag{13}$$

In the case of unoriented shear flow, collisions taking place at $\alpha > \alpha_{cr}$ will be discarded from the analysis. For shear flow with periodic flow reorientation, however, coalescence may still take place for $\alpha > \alpha_{cr}$. If drainage takes place rapidly, virtually all collisions end in coalescence. In this case, the

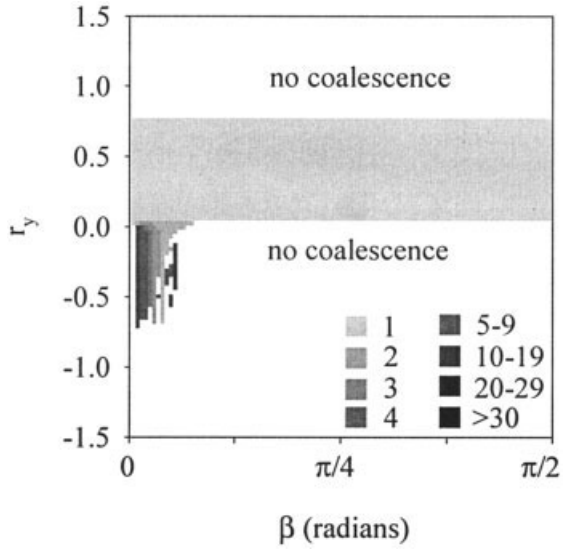

Figure 4. Number of reorientation periods (gray-scale code) necessary for coalescence $\gamma_T = 8\pi$, $\phi = 0.15$.

coalescence map does not differ much from the ones based solely on collision, for example, Figure 3a. Since drainage is a time-consuming independent step, the extent of coalescence zone is smaller than the zone of collision, as reflected in Figure 4. The value of critical angle, α_{cr} is found to be 50.5°, using $Ca = 1$, $p = 0.6$, and $h_{cr}/R = 0.04$, which are typical for the experimental system of this study. The coalescence zone in Figure 4 is smaller than the collision zone in Figure 3a, as not all collisions end in coalescence. Additionally, flow reorientation taking place during drainage may also prevent droplet pairs from coalescing, as the drag force changes from being attractive to repulsive. The drag force is still attractive for droplet pairs with drainage time shorter than the time droplets are together before the next flow reorientation occurs. Therefore, in Figure 4, not only the extent of the coalescence zone is reduced with respect to the collision zone, but also for a part of the droplet positions r_y, coalescence is delayed with respect to collision, for example, larger numbers of periods are needed for coalescence.

Note that in each reorientation period, there are two flow reorientations as shown in Figure 2. It is seen that for a large value of γ_T, for example, 8 π, most droplets undergo coalescence before the flow is reoriented for the first time, and therefore, the zone where coalescence can take place is defined by the value of α_{cr} as in regular flows (Figure 5a). On the other hand, for $\gamma_T = \pi/2$ (Figure 5b), not all the droplet pairs can finish the drainage process before the next flow reorientation; in this case, the drainage process continues for several reorientation periods. Under these conditions, the value of α_{cr} is no longer applicable, and the zone where collisions are effective is defined by the values of both α and β.

In order to visualize the effects of flow reorientation on mixing and coalescence in a system with multiple droplets, 10,000 massless tracer points — imitating the centers of the droplets – are placed in a periodic box. The shear flow undergoes the same reorientation as in Figure 2, and the trajectories of the tracer points are traced to generate Poincaré maps.[45] Poincaré maps for some values of $\gamma_T$for example, $\pi/2$, 2π and 8π, and for the values of $\beta = \pi/18$ and $\pi/90$, after 100 reorientation periods are presented in Figure 6. Some clustering is observed for $\gamma_T = \pi/2$ (Figure 6a and d) reflecting poor mixing. The tracers are more uniformly mixed with the increase of γ_T to 2π, and 8π. The bands seen in Figure 6e are the result of simple shear flow. The existence of zones with very high concentration of material points in the form of spots (Figures 6a,b, and d) or bands (Figure 6e), indicates that droplet separation is drastically reduced due to increased local droplet concentration. Thus, under these conditions, the possibilities of droplet collision and subsequent coalescence are substantially increased. At higher values of γ_T, for example, 8π, the material points are more uniformly separated, for example, in Figures 6c and f. Therefore, the separation between two neighboring droplets becomes larger, thus, reducing the possibilities of collision and coalescence. In view of this, one

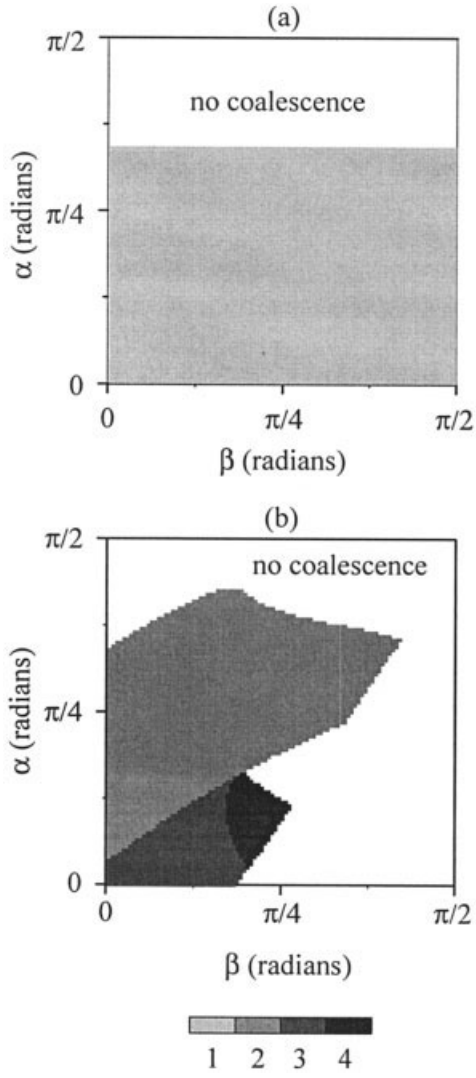

Figure 5. Number of flow reorientations to effect coalescence (grayscale) as function of the collision angle, α, and reorientation angle, β. Ca = 1, p = 0.6, and $h_{cr}/R = 0.04$.

(a) $\gamma_T = 8\pi$, and (b) $\gamma_T = \pi/2$.

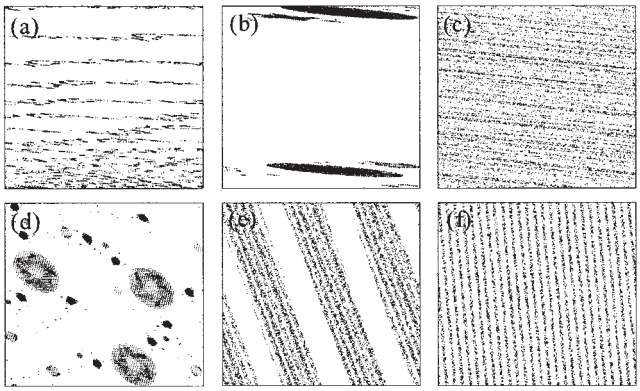

Figure 6. Poincaré maps generated from particle trajectories in a periodic box.

(a) $\gamma_T = \pi/2$, $\beta = \pi/18$, (b) $\gamma_T = 2\pi$, $\beta = \pi/18$, (c) $\gamma_T = 8\pi$, $\beta = \pi/18$, (d) $\gamma_T = \pi/2$, $\beta = \pi/2$, (e) $\gamma_T = 2\pi$, $\beta = \pi/2$, and (f) $\gamma_T = 8\pi$, $\beta = \pi/2$.

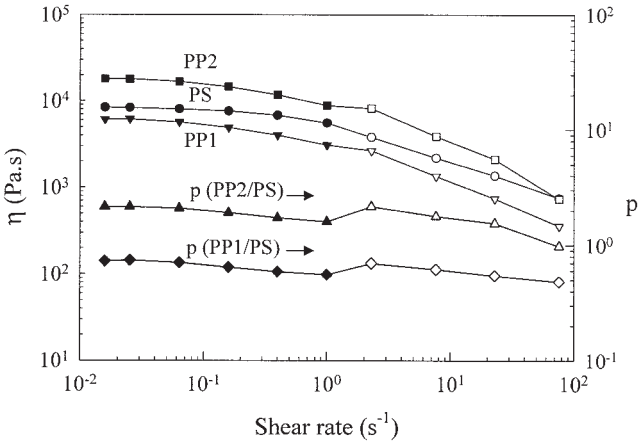

Figure 7. Steady-state viscosity and viscosity ratio vs. shear rate for PP1, PP2, and PS.

Filled symbols correspond to data from cone and plate rheometer and open symbols from capillary rheometer.

may expect that under the conditions of uniform mixing, for example, for $\gamma_T = 8\pi$, the fraction of droplets undergoing coalescence is greatly reduced, for example, compared to poor mixing observed for $\gamma_T = 2\pi$ and $\gamma_T = \pi/2$. Note, however, that collision frequency and the number of effective collisions between two droplets are higher for $\gamma_T = 8\pi$ than other cases (Figure 3b) for the same droplet concentration. Nevertheless, coalescence is suppressed under this condition due to lower local droplet concentrations and delayed drainage, especially at higher values of β. At smaller values of γ_T, poor mixing results, leading to the formation of zones of high droplet concentration which favor coalescence. This analysis will be used in the interpretation of experimental results, although the shear rate varies in both space and time in most experimental chaotic mixers, thus, subjecting droplet pairs to sequences of strong and weak flows.

Experimental

Materials and blending

Immiscible polymer blends were prepared in our laboratory using polystyrene (PS, Styron® 685, Dow Chemical, glass-transition temperature 108°C) as the continuous phase. Two grades of polypropylene with melt flow indices of 5.1 (PP1, Equistar Chemical, PP8000GK) and 0.7 (PP2, Equistar Chemical, PP31S07A), respectively, were selected as the dispersed phase. The value of interfacial tension for PS/PP system at 220°C was approximately 0.005 N/m.[46] The values of steady shear viscosity of the polymers at 220°C are reported in Figure 7. The values of zero-shear viscosity ratio (p) for PP1/PS and PP2/PS blends were, respectively, 0.6 and 1.9. A 25 mm dia. cone and plate rheometer (ARES) was used for shear rates lower than 1 s^{-1} (filled symbols in Figure 7) and a capillary rheometer (Instron, dia. of 1.5 mm, length-to-dia. ratio of 28.5) was used for shear rates ranging from 1 to 100 s^{-1} (open symbols in Figure 7). Polymer blends for coalescence experiments were prepared by mixing the polymers with compositions, 10/90, 15/85, and 20/80 by volume, respectively of PP and PS in a 30 mm Werner-Pfleiderer corotating twin-screw extruder. The mean value of shear rate was calculated to be 50 s^{-1}, assuming filled screw channel.

Chaotic mixing

A chaotic mixer consisting of two rolls rotating in an eight-shaped chamber as shown in Figure 8 was used in experiments. A more detailed description of the experimental setup is provided elsewhere.[12] Chaotic fluid element trajectories were generated using a sine waveform for rotor motion

$$\Omega_1(t) = \Omega_0\left(1 + \cos\frac{2\pi}{T}t\right) \tag{14}$$

$$\Omega_2(t) = \Omega_0\left(1 - \cos\frac{2\pi}{T}t\right) \tag{15}$$

where $\Omega_i(t)$ is the angular velocity of the rotor i = 1,2 at any time t, Ω_0 is a reference angular velocity, and T is the period of oscillation. The sine waveform produced more uniform droplet-size distribution (DSD) than the square and steady waveforms.[11] Different degrees of chaotic mixing were produced by changing the value of angular displacement per period (θ), between $\pi/2$ and 8π; θ is defined as

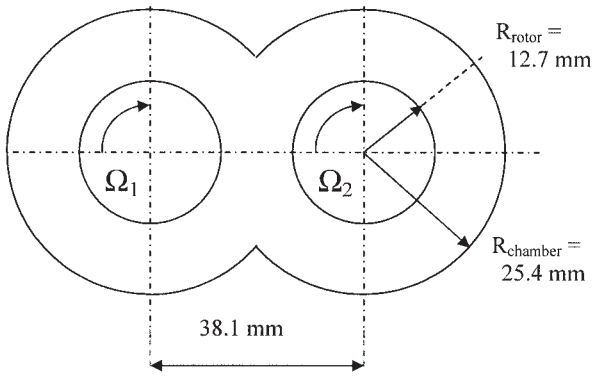

Figure 8. Chaotic mixer.

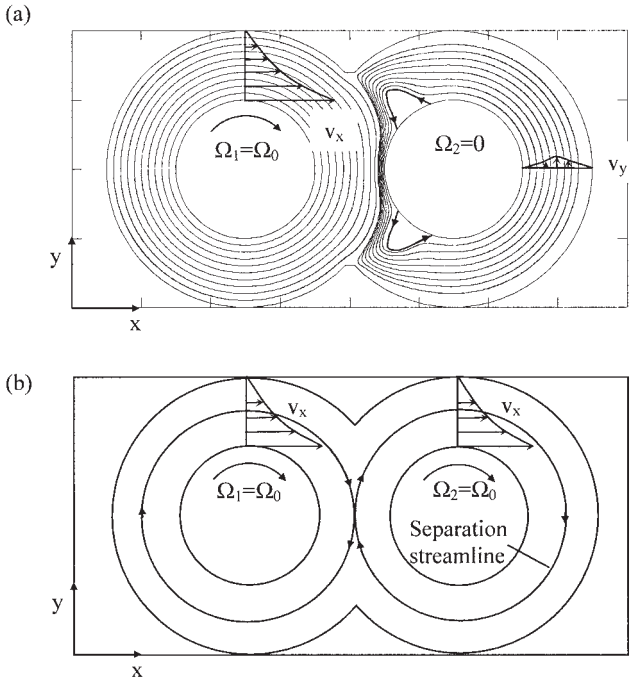

Figure 9. Streamlines and velocity profiles.

(a) With only left rotor in motion, (b) both rotors in motion at the same speed. The coordinate axes are represented by x and y. The x- and y-directional velocities are represented by, respectively v_x and v_y.

$$\theta = \int_0^T \Omega(t)dt \tag{16}$$

and its value for the sine waveform was calculated from $\theta = \Omega_0 T$. Although the time-averaged shear rate at the rotor surface was approximately 4 times that at the chamber wall for the mixer geometry presented in Figure 8, a value of mean shear rate ($\dot{\gamma}_{mean}$) in the mixer was calculated from the expression in Eq. 17 for the purposes of comparison of the experimental results. Note that the values of ($\dot{\gamma}_{mean}$) fell between the shear rates at the rotor surface and the chamber wall

$$\dot{\gamma}_{mean} = \frac{\Omega_0 R_{rotor}}{R_{chamber} - R_{rotor}} \tag{17}$$

In view of this, the term θ assumed the same significance as the parameter γ_T used in Figures 3 – 6. Figure 9 presents representative steady streamline portraits and sketches of steady velocity profiles obtained by boundary integral method.[12] Note that due to steady motion of the rotors, a majority of fluid elements travel on "circular trajectories" (Figure 9a) around the rotors and do not mix well. These trajectories become chaotic with time-periodic speed variation as given in Eqs. 14 and 15.

Blends prepared by twin-screw extruders were allowed to melt in the mixing device for a period of 10 min at 220°C before chaotic mixing began. An independent experiment showed that no significant coalescence of PP-droplets was observed during this period. The molten polymers were mixed at 220°C up to 3,000 s at $\dot{\gamma}_{mean}$ = 0.3, 0.5, 0.8, and 1.4 s^{-1}, after which the materials were solidified using ice-water bath. Under these conditions, the PP-phase cooled to well below its melting point in approximately 30 s. The morphology did not change significantly during this step. The entire material was cooled to room-temperature in approximately 5 min.

Droplet size analysis

The solidified materials from the chaotic mixer were ground into approximately 1 mm granules and a small portion (approximately 0.5 g) was subjected to Soxhlet extraction for 24 h using toluene to remove the PS-phase and to recover the PP-droplets in a ceramic thimble of 0.1 μm nominal pore size (Alundum AN889, Saint-Gobain). The PP-droplets, obtained in the form of "cake", were dried at 70°C for 24 h under high vacuum, sputtered with silver alloy, and imaged in a scanning electron microscope (SEM, Hitachi S-2150). The droplet-size distribution (DSD) was generated from the measurement of the diameter of at least 1200 droplets using Scion Image software (Beta 4.0.2. Scion Corporation, www.scioncorp.org). The values of number average (D_n) and volume average (D_v) diameter were calculated from the following expressions

$$D_n = \frac{\sum n_i d_i}{\sum n_i} \tag{18}$$

$$D_v = \frac{\sum n_i d_i^4}{\sum n_i d_i^3} \tag{19}$$

where n_i is the number of droplets with dia. d_i.

Results and Discussion

Evolution of DSD due to coalescence

The evolution of DSD of PP1/PS 10/90, 15/85, and 20/80 blends sheared at $\dot{\gamma}_{mean}$ = 0.8 s^{-1} with a value of $\theta = 8\pi$ are presented in Figure 10. For PP1/PS 10/90 blend, appreciable droplet coalescence is observed, and the initially sharp DSD became broader and shifted toward larger sizes, as shown in Figure 10a. Comparing the DSD at 1,800 s with that at 1,200 s in Figure 10a, it is apparent that at later times, only the smaller droplets continued to undergo coalescence and larger droplets, formed early on, did not go through much coalescence at later periods. A pseudo-steady-state droplet-size distribution (SSD) was reached after 1,800 s of shearing, after which time coalescence of even the smaller droplets slowed down significantly. Similar behavior was observed for the other compositions of the same blend as in Figures 10b, and c. Note that in each case, the initial, narrow DSD, shifted to broader distributions with larger droplets. In addition, SSD was reached faster for blends containing higher fractions of PP due to higher frequency of collision as in Eq.1; in Figure 10c, for example, SSD was reached only after 600 s of shearing. An almost time-invariant distribution of the droplets of larger diameter can be rationalized based on longer drainage times required for further coalescence of larger droplets.[42] For coalescence of large droplets, the evolution of DSD is dictated by a slow drainage step and drainage time is independent of the volume fraction (see Eqs. 7 – 11). At longer shearing times, the distribution remains practically unchanged, thus generating a

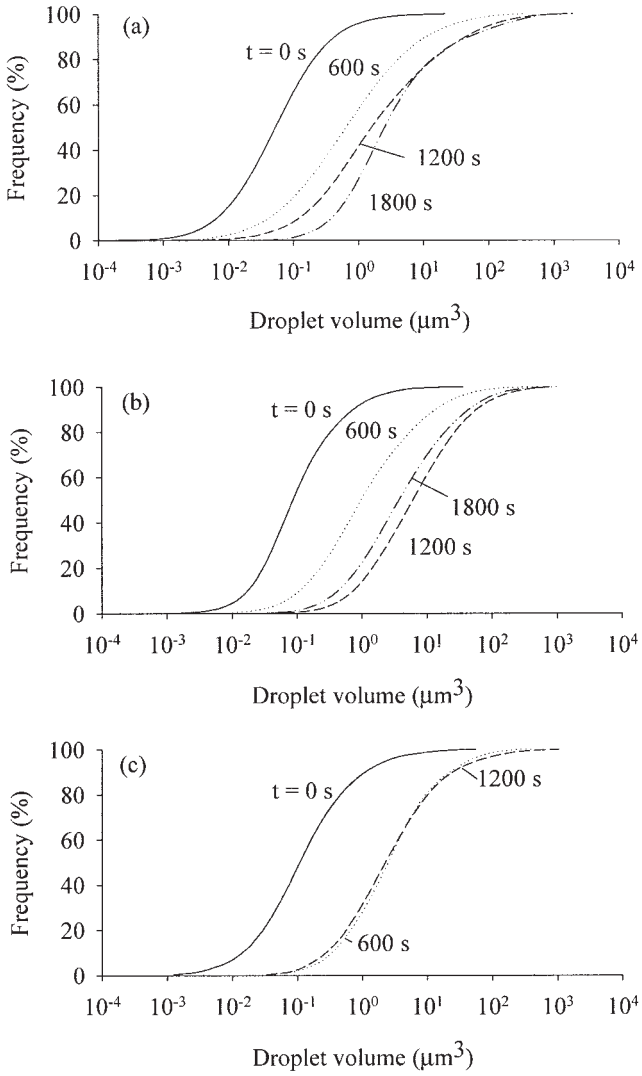

Figure 10. Evolution of DSD for PP1/PS.

(a) 10/90, (b) 15/85, (c) 20/80 blends, sheared at $\dot{\gamma}_{mean} = 0.8$ s^{-1}, and $\theta = 8\pi$.

SSD. The same observation was made in this study involving experiments with steady shearing motion of the rotors. This is in line with the results of other investigators.[47-49] Rother and Davis[41] predicted a monodisperse DSD with drop size much larger than the initial size at very long shearing times. The SSD observed in Figure 10 were far from monodisperse, may be due to insufficient shearing time. However, shearing was not continued for longer than 30 min to prevent degradation of the polymers. Moreover, longer shearing times may not have yielded monodisperse DSD, as the flow pattern in the chaotic mixer itself was inhomogeneous.

One may also assume that some of the droplets in SSD shown in Figure 10 have resulted due to breakup of larger droplets formed early in the coalescence process. To verify if deformation and breakup of the droplets obscured the effects of coalescence, the value of critical capillary number in equation 1 was calculated from Figure 5 in Grace[7] using the value of viscosity ratio, p for the polymer system. It was found that droplets of dia. 1.7 μm ($D_c = 2R_c$) and smaller would not deform under the peak shear conditions at the rotor surface corresponding to $\dot{\gamma}_{mean} = 0.8$ s^{-1}. Accordingly, less than 5% of the droplets by number in the initial blends ($t = 0$) reported in Figure 10, were larger than D_c. In addition, the SSD shown in Figure 10 have about 50% of the droplets smaller than D_c. Thus, approximately 50% of the droplets in SSD, larger than D_c, were amenable to deformation and possibly breakup. However, conditions such as $Ca \gg Ca_c$ and $D \gg D_c$ must be met for breakup to occur in the timescale of typical coalescence experiments. Moreover, the shear rate in most regions of the mixer was considerably lower than the peak value of the shear rate used to compute Ca_c, as sinusoidal rotation pattern (Eqs. 14, 15) was used. Therefore, the SSD for the blends shown in Figure 10 reflect mostly the effects of droplet coalescence and not breakup.

Effect of θ

It was indicated earlier that θ was a measure of the degree of chaotic mixing. At larger values of θ, say $\theta = 8\pi$ radians, almost all fluid elements in the system had chaotic trajectories and better mixing was produced. On the other hand, for $\theta = 2\pi$ radians, approximately 2/3 of the fluid elements experienced chaotic motion.[12] For even smaller values of θ, for example, $\theta = \pi/2$, the zone experiencing chaotic motion would be negligible and other effects would be stronger, as discussed later.

The experimental system differed from the model chaotic flow used in Figures 3 – 6 in the following aspects — in experiments, the shear rate varied in both space and time. Thus, there was a distribution of reorientation periods, reorientation angles, and shear rates across the gap of the mixer. Nevertheless, the conclusions obtained from Figures 3 – 6 can be used to interpret many of the experimental findings. Figure 11 shows the SSD corresponding to PP1/PS 15/85 blend sheared at a mean shear rate of 0.8 s^{-1} with the values of θ ranging from $\pi/2$ to 8π. It is noticeable in Figure 11 that contrary to what was learned in Figure 10, the SSD differs even for the same concentration, for different levels of chaotic advection in the mixer. Increasing θ from 2π to 8π reduced the droplet sizes in the SSD. This fact is a clear indication of reduction in droplet coalescence with the increase of degree of chaotic mixing in the mixer. It was seen in Figure 5 that for values of γ_T between 2π and 8π, no value of β totally suppressed droplet collision. Also, as γ_T was increased, the collision frequency approached

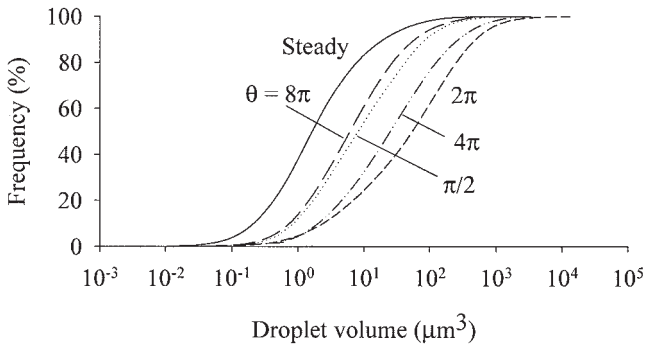

Figure 11. Effect of θ on the SSD for PP1/PS 15/85 blends sheared at $\dot{\gamma}_{mean} = 0.8$ s^{-1}

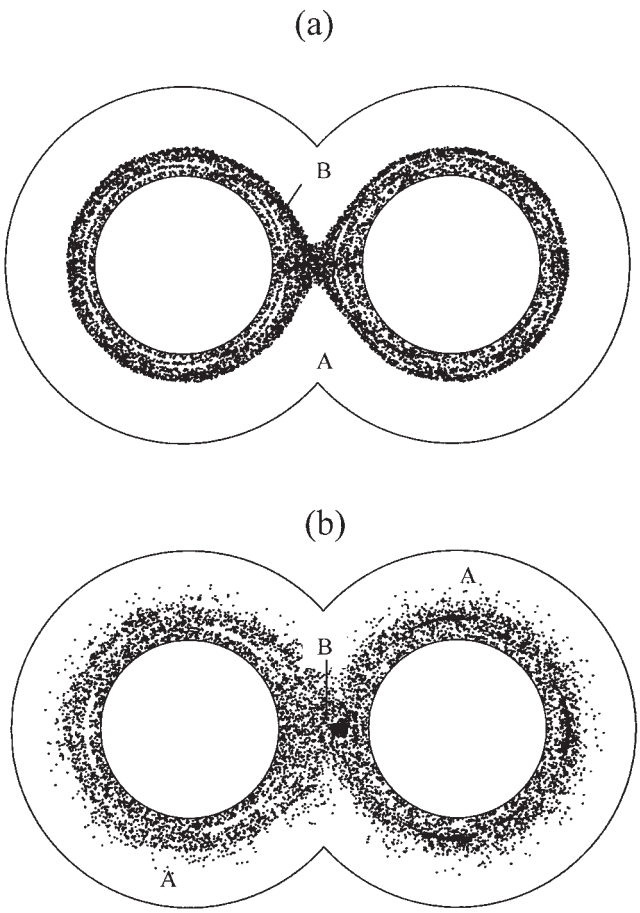

Figure 12. Poincaré maps for, (a) $\theta = \pi/2$, and (b) $\theta = \pi$.

Fluid elements follow circular trajectories in the zones labeled A.

that of unoriented flow ($\beta = 0$). On the other hand, under conditions of good mixing, for example, at higher values of γ_T, the droplets had to travel larger distances in order to undergo collision. Therefore, low values of θ, which generated poor mixing conditions, also reduced the chances of coalescence, as seen in Figure 11 for $\theta = \pi/2$. Reduced coalescence was also observed in the case of steady rotor motion. In this case, droplets followed circular trajectories and traveled large distances before undergoing collision. However, in mixing operations, time-invariant flow field is rarely used. The reduced coalescence seen in Figure 11 for $\theta = \pi/2$ can be attributed to circular trajectories of most fluid elements (those in zone A) except for the zones near the center of the mixer (zone B), as revealed by the Poincaré map in Figure 12a. The circular trajectories in this case refer to fluid elements traveling around the rotors, without much mixing with the rest. Note that overall mixing performance is poor under this condition, both due to circular trajectories in zone A and KAM surfaces in zone B. Figure 12b shows that mixing improved somewhat for $\theta = \pi$, and best mixing was obtained for $\theta = 8\pi$,[12-13] the same condition, showing significant reduction of coalescence in Figure 11. Therefore, chaotic mixing not only expedites size reduction and morphology development during mixing of polymers in chaotic mixers,[12, 15] but also reduces droplet coalescence due to frequent flow reorientation experienced by a large body of the fluid in chaotic mixers.

Effect of shear rate

Although the results reported in Figures 3 and 4 and associated discussions involved constant values of γ_T, shear rate was included in the factor $\gamma_T \equiv \dot{\gamma}\tau$ in Eqs. 2 – 5, and its influence on the rate of collision can now be evaluated. For a given value of γ_T, more collisions are expected at higher shear rate. In addition, shear rate influences the drainage rate, as it appears in the expression of capillary number, *Ca* in Eq. 9. An immediate impact of increased shear rate is reduced contact time (Eq. 8) and, consequently, collisions become less efficient at higher shear rates. Figure 13 shows the values of D_n and D_v as function of $\dot{\gamma}_{mean}$ obtained from the SSD for PP1/PS 15/85 blend. A decrease in droplet size is observed as $\dot{\gamma}_{mean}$ was increased from 0.3 s^{-1} to 0.5 s^{-1}. In this case, the value of *Ca* increased with shear rate and the efficiency of droplet coalescence reduced. However, for the same initial blend sheared at $\dot{\gamma}_{mean} = 0.8\ s^{-1}$, Figure 13 shows an increase in droplet diameter, over those for $\dot{\gamma}_{mean} = 0.3\ s^{-1}$ and 0.5 s^{-1}. This is certainly an unexpected trend, and is not restricted only to the chaotic flow. The same trend was observed with steady rotor motion when the value of $\dot{\gamma}_{mean}$ was increased to 1.2 s^{-1}. A simple calculation based on simple shear flow can be invoked to compute the values of C_{eff} (Eq. 13), the frequency of collisions leading to coalescence as function of shear rate. In these calculations, a value of $h_{cr}/R = 0.009$ was used. The results depicted in Figure 14 shows that the value of C_{eff} increases with shear rate — due to increased value of C — until a critical value of shear rate, beyond which the value reduces rapidly to zero. In the latter case, P_{12} decreases rapidly with shear rate as the contact time is not enough for completion of the drainage step. In view of this, it can be inferred that droplet coalescence occurs faster at high rates of shear and, therefore, the pseudo-steady state droplet-size distributions are obtained

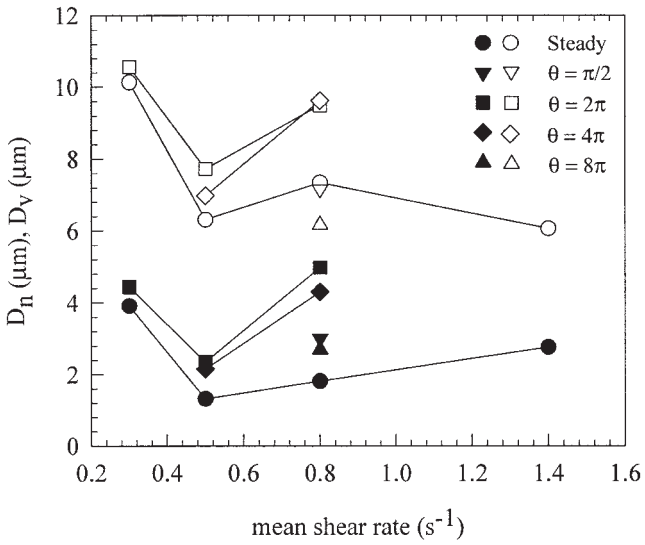

Figure 13. Average droplet diameters, D_n (filled symbols) and D_v (open symbols), for PP1/PS blends 15/85 as function of the shear rate.

The total time of shearing was 1,800 s.

more rapidly. On the other hand, at low shear rates, the SSD is approached slowly. In view of this and that the same maximum shearing time of 30 min was used in each case, it can be inferred that in Figure 13, the values of D_n and D_v for $\dot{\gamma}_{mean} \geq 0.8\ s^{-1}$ represent SSD, while those corresponding to $\dot{\gamma}_{mean} = 0.3\ s^{-1}$ and $0.5\ s^{-1}$ did not fully reach the pseudo-steady-state distributions. This kinetic effect affected the outcome of both chaotic flow and the flow with steady rotor motion. In view of the trend seen in Figure 13, one may wonder if D_n should continually increase with $\dot{\gamma}_{mean}$. As evident in Figure 14, the drainage step becomes rate determining and most collisions are not effective at higher shear rates. Note that the trend shown in Figure 14 was generated using an initial droplet radius of 0.35 μm and the properties of the polymer used in experiments. Therefore, coalescence is subdued at high rates of shear. The value of shear rate, beyond which coalescence would be subdued for this system, was not explored in this study.

Effect of viscosity ratio

The effect of viscosity ratio was studied by considering two grades of PP — PP1 and PP2 — which offered viscosity ratio (p) of, respectively 0.6 and 1.9. These values remained approximately constant for the range of shear rates involved in the experiments. Figures 15a,b present the evolution of D_n for PP1/PS 15/85 and PP2/PS 15/85 blends sheared at $\dot{\gamma}_{mean} = 0.3\ s^{-1}$ in steady flow and at $\dot{\gamma}_{mean} = 0.8\ s^{-1}$ in chaotic flow with $\theta = 8\pi$. Comparing the values of D_n for two blends, it is seen that initially (< 600 s) the rate of coarsening is similar for both PP1/PS and PP2/PS blends (see also Figure 14). At short shearing times, the efficiency of effective collisions was relatively high and the rate of coarsening was controlled by the collision frequency. As the droplet sizes increased at later times, the coalescence process was controlled by the drainage step. The film drainage was more retarded in the case of higher viscosity droplets. Consequently, for the same collision frequency, coalescence was drastically reduced as p was increased from 0.6 to 1.9. Accordingly, the SSD was achieved faster

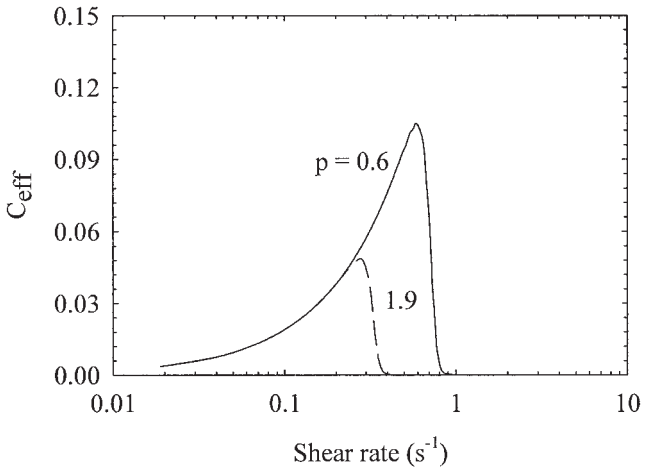

Figure 14. Frequency of effective collisions, C_{eff}, as function of the shear rate for two values of viscosity ratio.

$\eta_c = 7600$ Pa.s, $\Gamma = 0.005$ N/m, $\phi = 0.15$, A = 10^{-20} Joule, R = 0.35 μm.

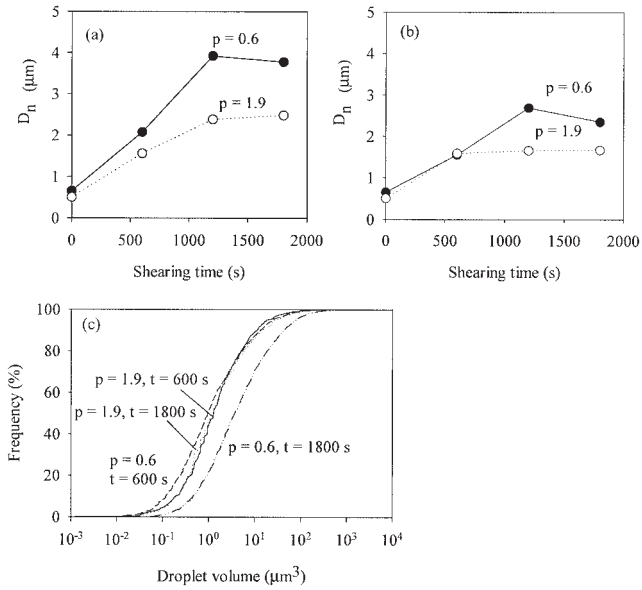

Figure 15. Effect of the viscosity ratio on the droplet size evolution for PP1/PS 15/85 (filled symbols) and PP2/PS 15/85 (open symbols).

(a) $\dot{\gamma}_{mean} = 0.3\ s^{-1}$, steady; (b) $\dot{\gamma}_{mean} = 0.8\ s^{-1}$, $\theta = 8\pi$; and (c) Droplet-size distributions $\dot{\gamma}_{mean} = 0.8\ s^{-1}$, $\theta = 8\pi$.

(Figure 15c) with lower values of D_n (Figure 15a, b) for the blends with higher viscosity ratio p.

Concluding remarks

This study showed that time-periodic flow reorientation mechanism present in chaotic mixing devices can substantially reduce coalescence of droplets of immiscible polymer blends. Frequent flow reorientations alter the droplet trajectories and, therefore, alter both collision frequency and interaction times between the droplets. Such information can be used in the development of better designs of chaotic mixing devices, and for optimization of modular mixing elements, such as those used in twin-screw mixers where the objective is to produce and retain the fine-scale dispersed phase morphology. The study also showed that fluid drainage becomes a controlling factor beyond a critical shear rate, for larger droplets, and for higher viscosity droplets. In these cases, coalescence is substantially retarded.

Acknowledgments

Financial support provided by National Science Foundation CAREER program (DMI-0134106) is gratefully acknowledged. JEP is grateful for study leave granted by National University of Colombia, Bogota, Colombia.

Literature Cited

1. Utracki LA. Polymer alloys and blends: thermodynamics and rheology. New York; Oxford University Press; 1990.
2. Lyngaae-Jørgensen J. Experimental methods for *in situ* studies of morphology development during flow: The case of instability of thin films studied by light scattering. *J Macromol Sci Phys*. 1996;B35:357-373.
3. Lindt JT, Gjosh AK. Fluid mechanics of formation of polymer blends.

Part I. Formation of lamellar structure. *Polym Eng Sci*. 1992;32:1802-1813.
4. Scott CE, Macosko CW. Model experiments concerning morphology development during the initial stages of polymer blending. *Polymer*. 1995;36:461-470.
5. Sundararaj U, Macosko CW, Rolando RJ, Chan HT. Morphology development in polymer blends. *Polym Eng Sci*. 1992;32:1814-1823.
6. Sundararaj U, Dori Y, Macosko CW. Sheet formation in immiscible polymer blends: model experiments on initial blend morphology. *Polymer* 1995;36:1957-1968.
7. Grace HP. Dispersion phenomena in high viscosity immiscible fluid systems and application of static mixers as dispersion devices in such systems. *Chem Eng Comm*. 1982;14:225-27
8. DeRoussel P, Khakhar DV, Ottino JM. Mixing of viscous immiscible liquids. Part 2. Overemulsification-interpretation and use. *Chem Eng Sci*. 2001;56:5531-5537.
9. Ramic AJ, Hudson SD, Jamieson AM, Manas-Zloczower I. Temporary droplet-size hysteresis in immiscible polymer blends. *Polymer*. 2000; 41:6263-6270.
10. Minale M, Mewis J, Moldenaers P. Study of the morphological hysteresis in immiscible polymer blends. *AIChE J*. 1998;44:943-950.
11. Jana SC, Sau M. Effects of viscosity ratio and composition on development of morphology in chaotic mixing of polymers. *Polymer*. 2004; 45:1665-1678.
12. Sau M, Jana SC. A study on the effects of chaotic mixer design and operating conditions on morphology development in immiscible polymer systems. *Polym Eng Sci*. 2004;44:407-422; Errata: *Polym Eng Sci*. 2004;44,1403.
13. Sau M, Jana SC. Effect of waveforms on morphology development in chaotic mixing of immiscible polymers. *AIChE J*. 2004;50:2346-2358.
14. Zumbrunnen DA, Inamdar S. Novel sub-micron highly multy-layered polymer films formed by continuous flow chaotic mixing. *Chem Eng Sci*. 2001;56:3893-3897.
15. Zumbrunnen DA, Chhibber C. Morphology development in polymer blends produced by chaotic mixing at various compositions. *Polymer*. 2002;43:3267-3277.
16. Kwon O, Zumbrunnen DA. Progressive morphology development to produce multilayer films and interpenetrating blends by chaotic mixing. *J Appl Polym Sci*. 2001;82:1569-1579.
17. Jana SC, Ottino JM. Chaos-enhanced transport in cellular flows. *Phil Trans R Soc Lond A*. 1992; 338:519-532.
18. Nishimura T. Heat and mass transfer enhancement by chaotic mixing in laminar flow. *Trends Chem Eng*. 1994;1:199-214
19. Ganesan V, Bryden MD, Brenner H. Chaotic heat transfer enhancement in rotating eccentric annular-flow systems. *Phys Fluids.* 1997;9: 1296-1306
20. Metcalfe G, Ottino JM. Autocatalytic processes in mixing flows. Phys Rev. Lett. 1994;72:2875-2878.
21. Szalai ES, Kukura J, Arratia PE, Muzzio FJ. Effect of hydrodynamics on reactive mixing in laminar flows. *AIChE J*. 2003; 49:168-179
22. Chang HC, Sen M. Application of chaotic advection to heat transfer**.** *Chaos Solitons & Fractals*. 1994;4:955-975.
23. Kim S, Kwon T. Enhancement of mixing performance of single-screw extrusion processes via chaotic flows. Part I. Basic concepts and experimental study. *Adv Polym. Technol*. 1996;15:41-54
24. Jana SC, Scott E, Sundararaj U. Single extruder screw for efficient blending of miscible and immiscible polymeric materials, US Patent No. 6132076; 1998.
25. Chesters AK. The modeling of coalesce processes in fluid-liquid dispersions: A review of current understanding. *Trans I Chem E*. 1991;69A:259-270.
26. Janssen JMH, Meijer HEH. Dynamics of liquid-liquid mixing: A 2-zone model. *Polym Eng Sci*. 1995;35:1766-1780.
27. Fortelný I. Coalescence in polymer blends: Solved and open problems. *Macromol Symp*. 2000;158:137-147.
28. Fortelný I, éivný A. Film drainage between droplets during their coalescence in quiescent polymer blends. *Polymer*. 1998;39:2669-2675.
29. Yu W, Zhou C, Inoue T. A coalescence mechanism for the coarsening behavior of polymer blends during a quiescent annealing process. I. Monodispersed particle system. *J Polym Sci B Polym Phys*. 2000; 38:2378-2389.
30. Perilla JE, Jana SC. A time-scale approach for analysis of coalescence in processing flows. *Polym Eng Sci.* 2004;44:2254-2265.
31. Souza, A.M.C., Demarquette, N.R., Influence of coalescence and interfacial tension on the morphology of PP/HDPE compatibilized blends. *Polymer*. 2002:43:3959-3967.
32. DeRoussel P, Khakhar DV, Ottino JM. Mixing of viscous immiscible liquids. Part 1. Computational models for strong-weak and continuous flow systems. *Chem Eng Sci*. 2001;56:5511-5529.
33. Sundararaj U, Macosko CW. Drop breakup and coalescence in polymer blends: the effects of concentration and compatibilization. *Macromolecules*. 1995; 28:2647-2657.
34. Ottino JM, DeRoussel P, Hansen S, Khakhar DV. Mixing and dispersion of viscous liquids and powdered solids. *Adv Chem Eng*. 2000;25: 105-204.
35. Muzzio FJ, Ottino JM. Coagulation in chaotic flows. *Phys Rev A*. 1988;38:2516-2524
36. Aref H. Stirring by chaotic advection. J. Fluid Mech. 1984; 143:1-21.
37. Smoluchowski M. Mathematical theory of the kinetics of the coagulation of colloidal solutions. *Z Phys Chem*. 1917;92:129-168
38. Swanson PD, Ottino JM A comparative computational and experimental study of chaotic mixing of viscous fluids. *J Fluid Mech.* 1990;213: 227-249.
39. Leong CW, Ottino JM Experiments on mixing due to chaotic advection in a cavity. *J Fluid Mech*. 1989;209:463-499.
40. Jana, SC, Metcalfe, G, Ottino, JM Experimental and computational studies of mixing in complex Stokes flows: the vortex mixing flow and multicellular cavity flows. *J Fluid Mech*. 1994;269:199-246.
41. Rother MA, Davis RH. The effect of slight deformation on droplet coalescence in linear flows. *Phys Fluids.* 2001;13:1178-1190.
42. Bazhlekov IB, Chesters AK, van de Vosse FN. The effect of the dispersed to continuous-phase viscosity ratio on film drainage between interacting drops. *Int J Multiphase Flow*. 2000;26:445-466.
43. Allan RS, Mason SG. Particle motion in sheared suspensions XIV. Coalescence of liquid drops in electric and shear fields. *J Colloid Interface Sci*. 1962;17:383-408.
44. Hamaker HC. The London-van der Waals attraction between spherical particles. *Physica*. 1937;4:1058-1072.
45. Wiggins S. Global bifurcation and chaos: Analytical methods. New York: Springer; 1988.
46. Demarquette NR, Catelli de Souza AM, Palmer G, Macaubas PHP. Comparison between five experimental methods to evaluate interfacial tension between molten polymers. *Polym Eng Sci*. 2003;43:670-683.
47. Börshig C, Fries B, Gronski W, Weis C, Friedrich Ch. Shear-induced coalescence in polymer blends - simulations and rheo small angle light scattering. Polymer. 2000;41:3029-3035.
48. Lyu S, Bates FS, Macosko CW. Coalescence in polymer blends during shearing. *AIChE J*. 2000;46:229-238.
49. Vinckier I; Moldenaers P, Terracciano A, Grizzuti N. Droplet size evolution during coalescence in semi-concentrated model blends. *AIChE J*. 1998;44:951-958.

Manuscript received July 7, 2004, and revision received Dec. 29, 2004.